AUTO-DIAGNOSIS OF COVID-19 USING LUNG CT IMAGES WITH SEMI-SUPERVISED SHALLOW LEARNING NETWORK

Debanjan Konar
Department of Electrical Engineering,
Indian Institute of Technology Delhi
New Delhi, India

Bijaya Ketan Panigrahi
Department of Electrical Engineering,
Indian Institute of Technology Delhi
New Delhi, India

Siddhartha Bhattacharyya
Department of Computer Science and Engineering,
CHRIST (Deemed to be University), Bangalore, India
dr.siddhartha.bhattacharyya@gmail.com

Nilanjan Dey
Department of Information Technology,
Techno India College of Technology, Kolkata, India
Email:neelanjan.dey@gmail.com

Competing interests: The authors declare no competing interests.

June 10, 2020

ABSTRACT

Infection of Novel Coronavirus 2019 (COVID-19) on lung cells and human respiratory systems have raised real concern to the human lives during the current pandemic spread across the world. Recent observations on CT images of human lungs infected by COVID-19 is a challenging task for the researchers in finding suitable image patterns for automatic diagnosis. In this paper, a novel semi-supervised shallow learning network model comprising Parallel Quantum-Inspired Self-supervised Network (PQIS-Net) with Fully Connected (FC) layers is proposed for automatic segmentation followed by patch-based classifications on segmented lung CT images for the diagnosis of COVID-19 disease. The PQIS-Net model is incorporated for fully automated segmentation of lung CT scan images obviating pre-trained convolutional neural network models for feature learning. The PQIS-Net model comprises a trinity of layered structures of quantum bits inter-connected through rotation gates using an 8-connected second-order neighborhood topology for the segmentation of wide variation of local intensities of the CT images. Intensive experiments have been carried out on two publicly available lung CT image data sets thereby achieving promising segmentation outcome and diagnosis efficiency (F1-score and AUC) while compared with the state of the art pre-trained convolutional based models.

1 Introduction

The world has suffered a lot in the recent pandemic due to the 2019 novel coronavirus disease (COVID-19) since its rapid outbreak from Wuhan, China. There have been sharp rises in infected and suspected cases in almost all the countries in the world from the beginning of January 2020 as reported by World Health Organization [1]. The severe affect of coronavirus disease has inflicted a SARS-CoV-2 acute respiratory syndrome and has resulted in a new febrile respiratory tract illness. Despite imposition of various strict measures and physical isolation guidelines, the number of positive test cases is rising rapidly and as of today (22/05/2020), the total number of cases reported in the entire world is $5,329,268$ [2]. There are mainly three standard widely used diagnosis procedures viz. Reverse Transcription Polymerase Chain Reaction (RT-PCR) test from swab samples, Chest X-ray and Lung CT scan images for COVID-19 detection. However, the real-time RT-PRT test using detection of nucleotide has reported low sensitivity in China and hence it is not an effective tool for coronavirus infection detection [4] owing to lack of stability, quality and viral materials in specimens. In addition, lack of testing capabilities in the underdeveloped countries owing to insufficient test kits has spurred the demand for alternative COVID-19 diagnosis. The potential alternatives to RT-PRT test based COVID-19 detection are methods used on Lung CT scan image and Chest X-ray image segmentation. The captured lung CT scans of COVID-19 infected patients often show a bilateral patchy shadow. Moreover, Chest CT scan is a

noninvasive and a fast diagnosis procedure and reported high sensitivity for pre-screening of COVID-19 infections [4]. However, with rise in number of infections and suspected cases, it is a paramount and laborious tasks for the health experts to manually annotate the infected lesions and manual contour them in the current world-wide pandemic situation. In these circumstances, in order to maximize the diagnosis of the infected patients and to improve the treatment access, it is always preferred to have an automatic and robust segmentation technique followed by assessment of coronavirus infections.

1.1 Related Works

Recent years have witnessed the progress of deep learning technologies in the field of medical image segmentation which have become popular diagnostic tool due to key feature representation [5, 6, 7, 8, 9, 10]. In this year, a plethora of deep learning networks have been employed for automatic detection of COVID-19 pneumonia lung CT volumes and have reported promising accuracy [11, 12, 13, 14, 15]. A multi-objective differential evolution assisted convolutional neural network (CNN) [12] is suggested for COVID-19 lung CT image classification by leveraging the hyper-parameters of the CNN. Zheng *et al.* [16] proposed a weakly supervised deep learning model with the pre-trained U-Net for COVID-19 infection detection using lung CT volumes and reported high accuracy, sensitivity and specificity. Yan *et al.* [17] introduced a convolutional neural network introducing Progressive Atrous Spatial Pyramid Pooling to address the sophisticated infected lesions with overlapping and with wide variations of shape and orientation of lung CT volumes. However, owing to lack of sufficient annotated lung CT images and lack of image specific adaptability for unforeseen lung CT image classes (the infections on lung CT images vary with regions), pre-trained CNN models fail to achieve desired accuracy. In addition to this, requirement of high computational resources to train the aforementioned deeply supervised networks is seldom a cost effective solution for COVID-19 diagnosis. To avoid the over-fitting during training of CNN based models with small data sets, a latent representation learning exploring multiple features prevalent to lung CT volumes, is suggested by Kang *et al.* [15]. In addition to this, simple neural network model incorporating two coupled 3D Res-Nets with prior attention learning is proposed by Wang *et al.* [18]. In spite being relatively less complex models for COVID-19 infected lung CT image segmentation, these approaches rely on extensive feature learning during training.
In this article, we have proposed an integrated semi-supervised shallow learning network model comprising a Parallel Quantum-Inspired Self-Supervised Neural Network (PQIS-Net) followed by fully connected classification layers for COVID-19 diagnosis. Of late, the authors have proposed quantum-inspired self-supervised networks referred to as QIS-Net [19] and QIBDS Net [20] for automatic brain lesion segmentation. Authors have also developed the optimized version of QIBDS Net referred to as Opti-QIBDS Net [21] which is found suitable for brain tumor segmentation. These self-supervised network architectures which are tailored and tested on brain MR images and efficient in brain MR image segmentation serve as the inspiration behind the current work. In this manuscript, we aim to further investigate the parallel version of our proposed QIS-Net on COVID-19 infected lung CT images without any sort of supervision or training for segmentation followed by classification by fully connected layers for feasibility analysis on COVID-19 diagnosis.

1.2 Contributions

The four-fold significant contributions of the article are highlighted as follows:

1. Eventually, in the current pandemic situation in the world, it is an uphill task for the health care professionals to acquire large volumes of lung CT images with annotations for deep supervision. Hence, the primary focus of the paper is to offer a potential alternative to deeply supervised networks using a semi-supervised shallow neural network model composed of a fully parallel self-supervised network (PQIS-Net) for appropriate segmentation for tiny COVID-19 infected lesions and fully connected layer (FC layer) at the end for enabling training on weak data labels for suitable assessment of COVID-19 infections.
2. An 8-connected neighborhood topology-based segmentation using PQIS-Net for taking into cognizance the wide variations of local intensities of lung CT images, is the key contribution of the proposed work.
3. In addition, selections of p-random 2D patches from the PQIS-Net segmented images are allowed to augment the limited training data sets with high representation features to the constituent FC layers for processing (training) thereby obviating over-fitting.
4. Rigorous experiments have been carried out considering two different publicly available data sets of COVID-19 lung CT images, one purely for segmentation task and the other one for segmentation followed by classification to facilitate an accurate diagnosis. The extensive experimental results validate our proposed semi-supervised shallow neural network model which outperforms the state of the art pre-trained CNN models with weak annotations, thus promoting auto-diagnosis with self-supervised neural network models.

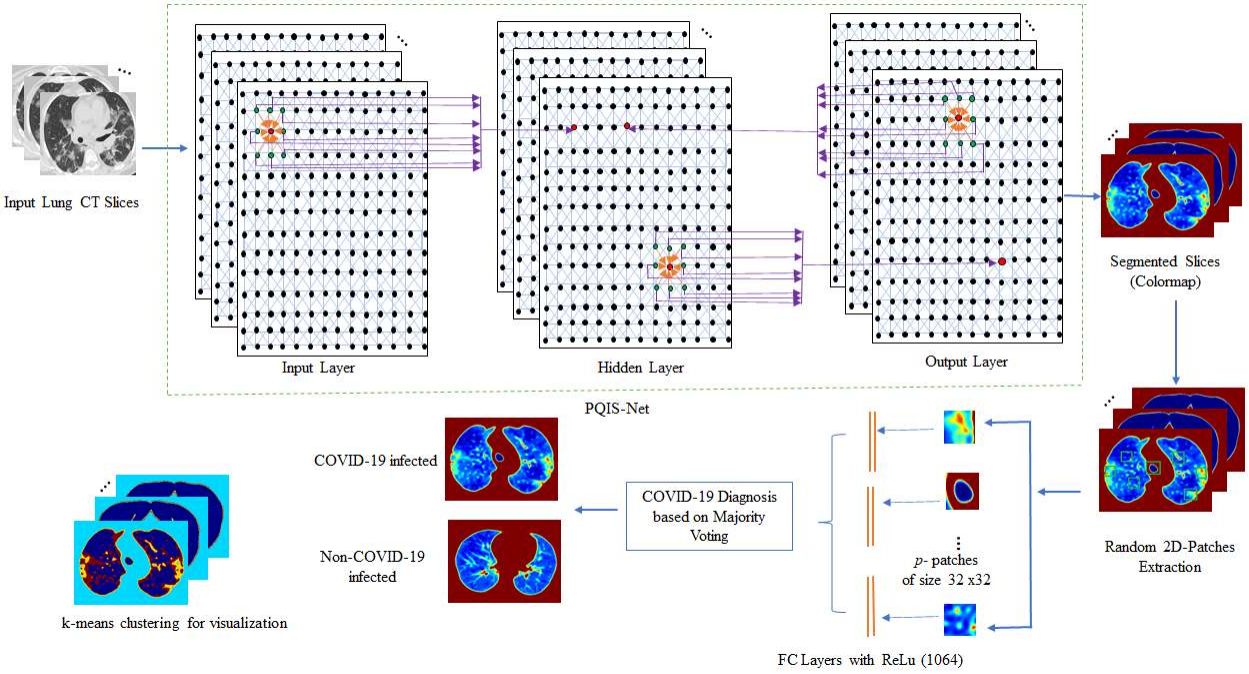

Figure 1: A parallel quantum-inspired self-supervised Network (PQIS-Net) assisted Semi-supervised Shallow Learning network for COVID-19 diagnosis (only three inter-layer connections are shown for clarity).

The remaining portion of the manuscript is organized as follows: The proposed semi-supervised shallow neural network model comprising PQIS-Net architecture and its operation with the fully connected layers are discussed in Section 2. Experimental results and discussions including the data set details, experimental setup is provided in Section 3. Finally, the concluding remarks are confabulated in Section 4.

2 Proposed Semi-supervised Shallow Neural Network model

The Parallel Quantum-Inspired Self-Supervised Neural Network (PQIS-Net) is the core of the proposed semi-supervised shallow neural learning model which is combined with fully connected layers at the end for classification and diagnosis of COVID-19 disease. The PQIS-Net is employed to segment lung CT image slices which are infected by COVID-19 or pneumonia in parallel fashion thereby reducing processing time. The PQIS-Net segmented images form highly representative features for classifications. An integrated semi-supervised shallow learning model incorporating the self-supervised PQIS-Net with Fully Connected (FC) layers at the end is targeted to develop which is appropriate for training at the FC layers with limited training data sets and can offer accurate diagnosis. The classification outcome is obtained using a majority voting scheme. A schematic outline of the proposed integrated self-supervised shallow neural network model with the fully connected layers is illustrated in Figure 1. The following subsection 2.1 sheds light on the detailed description of our previously developed quantum-inspired fully self-supervised neural networks [19, 20] and a short description about FC layers is also provided in subsection 2.2.

2.1 Parallel Quantum-Inspired Self-Supervised Neural Network (PQIS-Net) for Segmentation

The Parallel Quantum-Inspired Self-Supervised Neural Network is the extended version of our previous network architectures [19, 20] and comprises a trinity of layers of quantum neurons (represented as quantum bits or *qubits*). The incorporation of quantum-inspired computing in the suggested PQIS-Net stems from the fact that the classical self-supervised networks suffer from convergence problems [23, 24, 25]. The incorporation of quantum-inspired computing in the suggested parallel quantum-inspired self-supervised neural networks enables the faster convergence by reducing the number of epochs with forceful termination and hence yields better accuracy in segmentation tasks [19, 20, 21, 22, 26, 27]. The network dynamics of PQIS-Net replicates the basic operation of QIS-Net model [19] in parallel. The basis computation unit for the PQIS-Net is a quantum bit or a *qubit* designated by a quantum neuron in all trinity of layers in the architecture in matrix notation. One such layer matrix comprising *qubits* is shown out of the identical

parallel layers in the PQIS-Net, as follows.

$$\begin{bmatrix} |\phi_{11}^l\rangle & |\phi_{12}^l\rangle & |\phi_{13}^l\rangle & \dots & |\phi_{1m}^l\rangle \\ \dots & \dots & \dots & \dots & \dots \\ \dots & \dots & \dots & \dots & \dots \\ \dots & \dots & \dots & \dots & \dots \\ |\phi_{n1}^l\rangle & |\phi_{n2}^l\rangle & |\phi_{n3}^l\rangle & \dots & |\phi_{nm}^l\rangle \end{bmatrix}$$

Hence, each *qubit* is designated as ϕ_{ij}^l at the l^{th} layer of the network architecture. The network layers are inter-connected through 8-connected spatial neighborhood neuron subsets and serve as the significant characteristic of the network architecture. In each layer of the PQIS-Net architecture, quantum neurons are also intra-linked among themselves with intra-connection strengths $\frac{\pi}{2}$ (quantum 1 logic). The 8-connected neighborhood information of each candidate pixel is propagated to the subsequent layers for further computation in forward (input to hidden and hidden to output layer) and in counter-propagation fashions. The counter-propagation obviates the quantum back-propagation procedure thereby enabling faster convergence and reduced time complexity.
The principle of operation of the network is as follows: Each neuron of the network layers are designated as *qubits* or quantum bits and the inter-linked weights and its corresponding activation are mapped using rotation gates operating on the *qubits*. The classical input image pixels (x_i^l) at layer l are converted to quantum bits as

$$|\phi_i^l\rangle = \begin{bmatrix} \cos(\frac{\pi}{2}x_i^l) \\ \sin(\frac{\pi}{2}x_i^l) \end{bmatrix} i = 1, \dots m \times n \tag{1}$$

The rotation gates are employed to update the *qubit* with rotation angle for inter-connection strength and activation as ω^l and γ^l (say) at layer l, respectively. The angle of rotation of an interconnection strength, $\omega_{i,j}^l$ is decided by the relative difference measure between the candidate pixel (i) and its corresponding neighborhood (j) located at its 8-connected region in quantum formalism. The inspiration behind the adaptive relative measure in rotation angle evaluation is to distinct between the foreground and background image pixels. The angle of rotation is evaluated as

$$\omega_{i,j}^l = 1 - (\mu_i^l - \mu_{i,j}^l); i \in m \times n,\ j \in \{1, 2, \dots 8\} \tag{2}$$

Hence, the fuzzy graded input at the i^{th} candidate neuron and its corresponding spatially 8-connected second-order neighborhood neuron at layers l are μ_i^l and $\mu_{i,j}^l$, respectively. A single *qubit* is updated using a rotation gate with an angle ω^l as

$$\begin{bmatrix} \phi_{0'}^l \\ \phi_{1'}^l \end{bmatrix} = \begin{bmatrix} \cos(\frac{\pi}{2}\omega^l) & -\sin(\frac{\pi}{2}\omega^l) \\ \sin(\frac{\pi}{2}\omega^l) & \cos(\frac{\pi}{2}\omega^l) \end{bmatrix} \times \begin{bmatrix} \phi_0^l \\ \phi_1^l \end{bmatrix} \tag{3}$$

The fuzzy context sensitive activation in quantum formalism enables the bi-directional propagations (forward and counter propagations) is denoted at a layer l of a candidate neuron (pixel) i by ξ_i^l as

$$|\xi_i^l\rangle = \begin{bmatrix} \cos\gamma_i^l \\ \sin\gamma_i^l \end{bmatrix} \tag{4}$$

where, the angle of rotation for activation ξ_i^l is γ_i^l measured as the contribution of its 8-connected neighborhood neurons as follows

$$\gamma_i^l = 2\pi \times (\sum_j \mu_{i,j}^l) \tag{5}$$

The network input-output dynamics of a basic quantum neuron (i) in the self-supervised PQIS-Net is defined at the layer l as follows.

$$|y_i^l\rangle = \sigma_{PQIS-Net}(\sum_j^8 f(y_i^{l-1})\langle\varphi_j^l|\xi_j^l\rangle) \tag{6}$$

i.e.,

$$\begin{aligned} |y_i^l\rangle &= f(\frac{\pi}{2}\delta_i^{l-1} - \arg\{\sum_j^8 f(\omega_{j,i}^{l-1})f(y_i^{l-1}) - f(\xi_i^{l-1})\}) \\ &= \sigma_{PQIS-Net}(\sum_j^8 f(y_i^{l-1})\{cos((\omega_{j,i}^{l-1}) - \gamma_i^{l-1}) + \\ &\qquad \tau\ sin((\omega_{j,i}^{l-1}) - \gamma_i^{l-1}))\} \end{aligned} \tag{7}$$

Hence, the output at the i^{th} quantum neuron is depicted as y_i^l and the phase transformation parameters are denoted as δ_i^{l-1} (τ is an imaginary number).

$$\begin{aligned} |y_i^l\rangle &= \sigma_{PQIS-Net}(\sum_j^8 f(\frac{\pi}{2} y_j^l)\langle\varphi_{ji}^l|\xi_j^l\rangle) \\ &= \sigma_{PQIS-Net}(\sum_j^8 f(\frac{\pi}{2} \times \sigma_{PQIS-Net}(\sum_l^8 f(\frac{\pi}{2} y_j^l) \\ &\quad \langle\varphi_{kj}^l|\xi_k^l\rangle)\langle\varphi_{ji}^l|\xi_j^l\rangle) \end{aligned} \tag{8}$$

i.e.,

$$\begin{aligned} |y_i^l\rangle = \\ \sigma_{PQIS-Net}(\sum_j^8 f(\frac{\pi}{2} \times \sigma_{PQIS-Net}(\sum_k^8 f(\frac{\pi}{2} y_j^l)\cos(\omega_{kj}^l - \gamma_k^l) \\ \cos(\omega_{ji}^l - \gamma_j^l) + \tau \sin(\omega_{kj}^l - \gamma_k^l)\sin(\omega_{ji}^l - \gamma_j^l)))) \end{aligned} \tag{9}$$

The $\sigma_{PQIS-Net}$ activation function [Quantum Multi-level Sigmoidal (QMSig)] employed in the above Equation is defend as follows [19, 20].

$$\sigma_{PQIS-Net}(x; \lambda_\theta, s_\theta) = \sum_{\theta=1}^{L} \frac{1}{\lambda_\theta + e^{-\mu(x-(\theta-1)s_{\theta-1}-\xi)}} \tag{10}$$

where,

$$\lambda_\theta = \frac{S_N}{s_\theta - s_{\theta-1}} \tag{11}$$

Hence, the outcome of two adjacent classes viz., θ and $\theta - 1$ are s_θ and $s_{\theta-1}$ and the sum of the contribution of the 8-connected neighborhood pixels is designated as S_N. μ designates the steepness factor of the function and L is the number of gray levels in the segmented image.
The coherent network error cum loss function is introduced in the PQIS-Net and is evaluated as follows [19]:

$$\zeta(\omega, \gamma) = \frac{1}{2} \sum_k^S \sum_i^{m \times n} \sum_j^8 [\mathcal{W}_{i,j}^{\iota+1}(\omega_{i,j}, \gamma_i) - \mathcal{W}_{i,j}^{\iota}(\omega_{i,j}, \gamma_i)]^2 \tag{12}$$

where, $\mathcal{W}^{\iota}(\omega_{i,j}, \gamma_i)$ is the weighted inter-connection at a particular epoch ι and is linearly dependent on ω and γ. S is the number networks which constitute the PQIS-Net and is equal to number of image slices in a lung CT volume.

2.2 Fully-Connected (FC) Layers for Classification

The segmented lung CT images by PQIS-Net are targeted for classification using two Fully Connected (FC) layers to enable the diagnosis of COVID-19 or pneumonia (Non-Covid). However, to avoid over-fitting in the FC layers due to large size of segmented image features, patch-based classification is preferred incorporating p-number of random patches with relatively small size of 32×32 highly representative features. The center of the patches are randomly chosen to obviate the empty region of the segmented image. It may be noted that each image pixel of the p-random patches i considered as the highly representative features for classification. The value of p is chosen judiciously such that each pixel of the segmented CT image is considered at least once. Each path is fed to the FC layers for classification with a *Softmax* function and out of p-outcomes the final decision is made by a majority voting scheme [28]. Here, we have employed binary cross entropy loss for COVID-19 diagnosis. The loss ($\mathcal{L}_(w)$) is computed by leveraging the hyper-parameters w of the semi-supervised neural network model. It is defined as

$$\underset{w}{\operatorname{argmin}}\, \mathcal{L}_(w) = \sum_i^C [t_i \log y_(\alpha_i) + (1 - t_i) \log\{1 - y_(\alpha_i)\}] \tag{13}$$

where, $y(\alpha_i)$ is the predicted outcome by the FC layers on input α_i and with respect to the network parameter set w. t_i is the target output.

3 Results and Discussion

3.1 Data Set

Publicly available lung CT scan images are collected from two data sources [29, 30] and experiments are performed using the proposed semi-supervised neural network model on both the data sets. One of the data sets [29] contains total 2482 lung CT scans with variable sizes and out of these, 1252 lung CT scans are infected by COVID-19 and 1230 CT slices are not infected as COVID-19. The data set [29] is acquired from the real patients of Sao Paulo, City hospitals, Brazil. Another data set [30] comprises only 20 labelled COVID-19 lung CT volumes of fixed size 512×512 which includes infection masks, lung masks (left and right) and lung-infection pair masks. These labelled CT volumes are manually segmented and verified by radiologist experts. The data set [30] comprising the labelled CT volume masks are used in the experiment for the segmentation task. On the contrary, the other data set [29] is used for segmentation as well as classification tasks. Few samples from the Brazil data set [29] are shown in Figure 2 (COVID-19 infected) and in Figure 3 (non-COVID-19 infected).

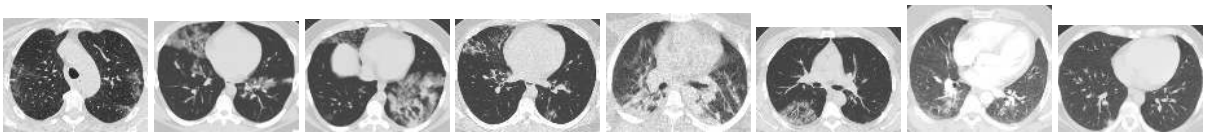

(a) #1 **(b)** #27 **(c)** #35 **(d)** #55 **(e)** #242 **(f)** #343 **(g)** #434 **(h)** #1212

Figure 2: COVID-19 infected input lung CT slices [29]

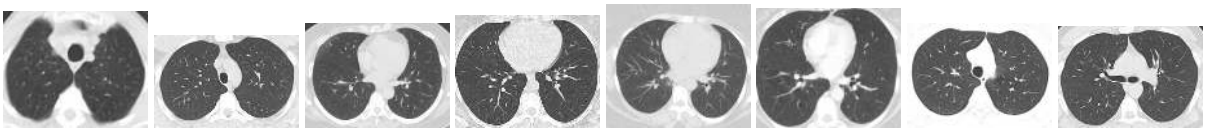

(a) #3 **(b)** #28 **(c)** #121 **(d)** #186 **(e)** #290 **(f)** #317 **(g)** #842 **(h)** #1217

Figure 3: Pneumonia (Non-Covid) infected input lung CT slices [29]

3.2 Experimental Setup

In this current work, extensive experiments have been carried out on lung CT images of variable sizes using high performance DL GPU (Nvidia RTX2070) System with MATLAB 2020a and Python 3.6.2 (Pytorch). The Brazilian data set [29] is divided into $7:3$ ratio for training and testing, respectively for segmentation followed by classification tasks. In addition, experiments are carried out using 5 and 10-fold cross validations separately. The results for these two different scenario are investigated by leveraging the set of hyper-parameters of the proposed semi-supervised shallow neural network.

The parallel quantum-inspired self-supervised network (PQIS-Net) is experimented with the pre-processed normalized gray-level CT scan images. Pre-processing of the input lung CT images from both the data sets [29, 30] are performed using normalization and standardization. The PQIS-Net segmented CT volumes are processed though the 2D binary masks available in the labelled CT volumes in the data set [30] to obtain the infected lesion on lung CT scans in the suggested semi-supervised model. The PQIS-Net is experimented with gray-level CT scan images using with distinct classes $L = 4, 5, 6, 7$ and 8 in optimized fashion [21]. In this experiment, the steepness (μ) in the $\sigma_{PQIS-Net}$ activation function, is varied in the range 0.230 to 0.240 with a step size 0.001. It has been observed that in majority cases, $\mu = 0.239$ yields the optimal segmentation.

The FC layers in the proposed semi-supervised shallow neural network model are rigorously trained using the stochastic gradient descent algorithm with a learning rate of 0.001. The convergence of accuracy and loss during training using the proposed semi-supervised shallow neural network is shown in Figure 4. In addition to this, experiments have been performed on two recently developed CNN architectures suitable for medical image segmentation viz., convolutional 3D-UNet [10] and Residual U-Net (ResNet50) [9] available in GitHub. The 3D-UNet and ResNet50 networks are rigorously trained using the *adam* optimizer with a learning rate of 0.0001 and a batch size of 32 allowing maximum 30 epochs to converge. The convergence of accuracy and loss during training using ResNet50 [9] are also demonstrated in Figure 5. The segmented output images resemble in size with the dimensions of the binary mask and the outcome 1 is considered as tumor region and 0 as background in detecting complete tumour. Pixel by pixel comparison with the manually segmented regions of interest or lesion mask allows to evaluate the dice similarity (DS) which is considered as

a standard evaluation procedure in automatic medical image segmentation. In addition to this segmentation, experiments are also set up for classifications the proposed Semi-supervised model, ResNet50 [9], 3D-UNet [10]. The other state of the art techniques include Kang *et al.* [15] and Wang *et al.* [18] for COVID-19 detection on the Brazilian data set [29]. The evaluation process involves the manually segmented lesion mask as ground truth and each 2D pixel is predicted as either True Positive (T_{RP}) or True Negative (T_{RN}) or False Positive (T_{RN}) or False Negative (F_{LN}).

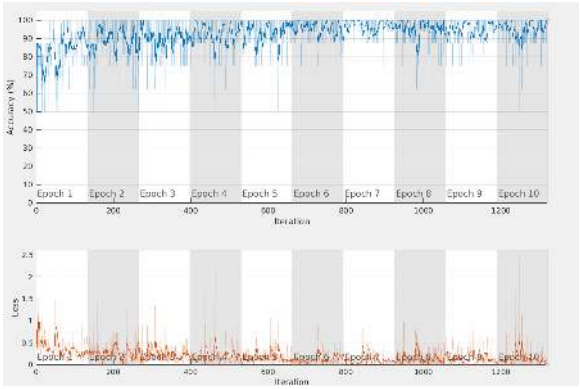

Figure 4: Convergence of the proposed semi-supervised shallow neural learning model allowing maximum 10 epochs during training with learning rate=0.001.

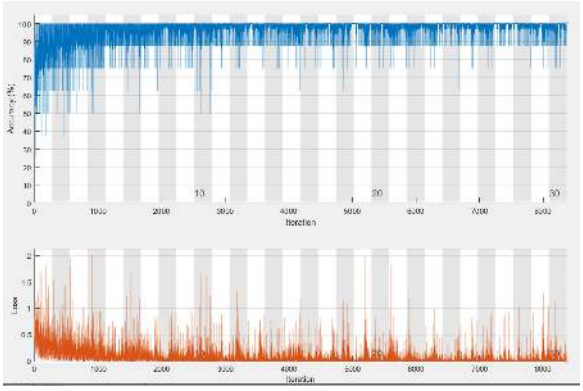

Figure 5: Convergence of the ResNet50 [9] model allowing maximum 30 epochs during training with learning rate=0.0001 and batch size =32

3.3 Experimental Results

Extensive experiments have been performed in the current setup and experimental outcomes are reported with the demonstration of numerical and statistical analyses on two different data sets [29, 30]. Segmentation using the proposed semi-supervised shallow neural network, pre-trained ResNet50 [9] and 3D-UNet [10] have been performed using both the data sets and segmentation performance is measured on data set [30] using evaluation metrics (ACC, DS, PPV, SS) [31]. The human expert (radiologist) segmented lung and infection masks lung CT image slices of size 512×512 are provided in Figure 6 with the input and the PQIS-Net segmented slice. The PQIS-Net is also tested on the Brazilian data set [29] and segmentation is performed on lung CT slices with two different classes (COVID-19 infected and non COVID-19 infected) as shown in Figure 7 and Figure 8, respectively. Table 1 reports the segmentation results of the proposed PQIS-Net with ResNet50 [9] and 3D-UNet [10] models for three different tasks (infection, lung, infection and lung). It is evident from the experimental data provided in Table 1 and from the statistical significance test (KS test) [19] conducted on the results that in spite of being a self-supervised network, the proposed PQIS-Net attains similar performance in segmentation tasks on the data set [30] in comparison with the pre-trained CNN models (ResNet50 [9] and 3D-UNet [10]) under the four evaluation parameters (ACC, DS, PPV, SS).

Table 2 presents the numerical results obtained using the proposed semi-supervised shallow neural network model, ResNet50 [9], 3D-UNet [10], Kang *et al.* [15] and Wang *et al.* [18] for COVID-19 detection on the Brazilian data

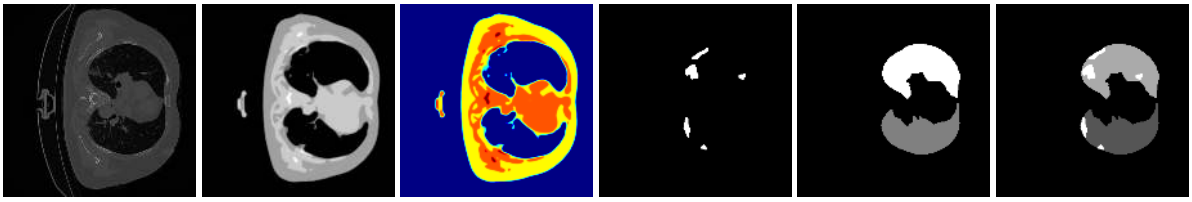

(a) Input **(b)** Segmented **(c)** Color-mapping **(d)** Infection mask **(e)** Lung mask **(f)** Infection & Lung mask

Figure 6: PQIS-Net segmented lung CT slice#171 [30] with the three different masks.

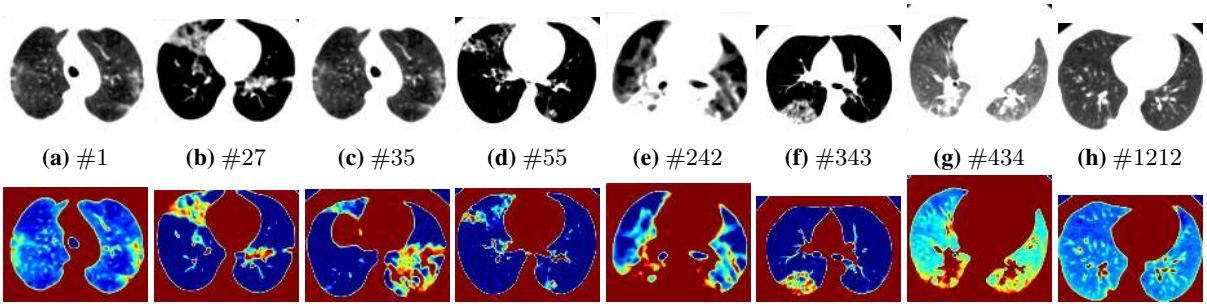

(a) #1 **(b)** #27 **(c)** #35 **(d)** #55 **(e)** #242 **(f)** #343 **(g)** #434 **(h)** #1212

(i) #1 **(j)** #27 **(k)** #35 **(l)** #55 **(m)** #242 **(n)** #343 **(o)** #434 **(p)** #1212

Figure 7: $(a-h)$ PQIS-Net segmented lung CT slices# [29] with COVID-19 infections followed by $(i-p)$ color mapping for class level $L=8$ with activation ξ

set [29]. The standard evaluation metrics used in Table 2 to measure the COVID-19 detection efficiency are accuracy, precision, recall, F1-score and AUC (Area under ROC curve) [31]. The convolutional based architectures (ResNet50 [9], 3D-UNet [10]) marginally outperform our proposed semi-supervised shallow neural network model in terms of accuracy. However, the proposed semi-supervised model report similar precision as ResNet50 [9] and 3D-UNet [10] and outperforms all four reported methods in terms of F1-score and AUC. In addition, the ROC curves and Confusion matrix representations for accuracy of COVID-19 detection are shown in Figure 9 and Figure 10, respectively. Moreover, to show the effectiveness of our proposed semi-supervised shallow neural network model, we have conducted one sided two sample Kolmogorov-Smirnov (KS) test with significance level $\alpha = 0.05$. It is interesting to note that in spite of being a semi-supervised shallow learning framework, the suggested semi-supervised model has shown similar accuracy (ACC) and F1-score compared with ResNet50 [9], 3D-UNet [10] and outperforms recent works on lung CT diagnosis proposed by Kang *et al.* [15] and Wang *et al.* [18]. Hence, it can be concluded, that the performance of the semis-supervised model on lung CT images is statistically significant and offers a potential alternative to the solution of deep learning networks and other time-intensive extensive features based learning paradigms in near future.

4 Conclusion

In this work, a novel attempt has been made using an integrated semi-supervised shallow neural network encompassing the parallel self-supervised neural network model (PQIS-Net) for fully automatic segmentation of lung CT images followed by fully connected (FL) layers for patch-based classification with majority voting. The PQIS-Net model incorporates the frequency components of the weights and inputs in quantum formalism thereby enabling faster convergence of the network states owing to reduction in computation. This intrinsic property of the PQIS-Net model yields precise and time efficient segmentation in real-time, which is evident from the results demonstrated in the experimental section on two different data sets in terms of accuracy, dice similarity, specificity and sensitivity for segmentation and accuracy, precision, recall, F1 score and AUC for classification in COVID-19 diagnosis. The proposed PQIS-Net is marginally under performs in lung CT image segmentation tasks by ResNet50 and 3D-UNet in terms of dice similarity. This is due to the fact that the proposed PQIS-Net is fully self-supervised neural network model based on pixel intensity based features. However, the proposed semi-supervised model outperforms all four state of the art methods in terms of F1-score and AUC for classification. Thus, the proposed parallel semi-supervised shallow learning model serves as an inspiration for promoting a potential alternative to the deep supervised learning frameworks for lung CT image segmentation for automatic COVID-19 diagnosis as well as for automatic medical image segmentation in

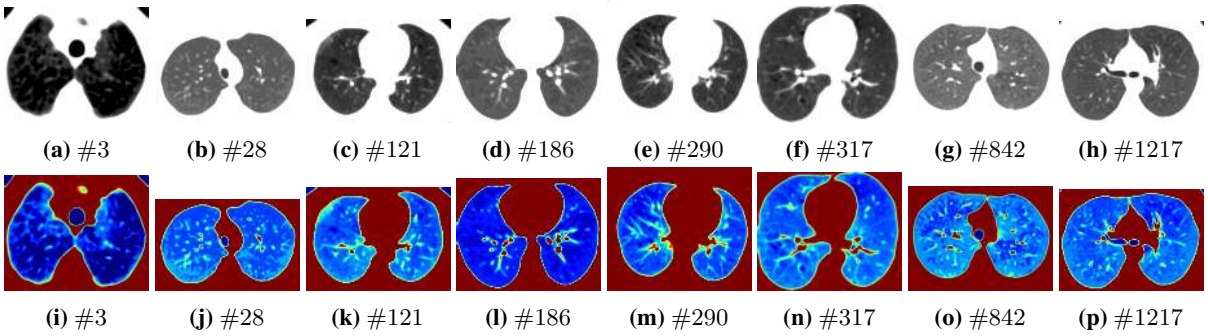

(a) #3 **(b)** #28 **(c)** #121 **(d)** #186 **(e)** #290 **(f)** #317 **(g)** #842 **(h)** #1217

(i) #3 **(j)** #28 **(k)** #121 **(l)** #186 **(m)** #290 **(n)** #317 **(o)** #842 **(p)** #1217

Figure 8: $(a-h)$ PQIS-Net segmented lung CT slices# [29] with Pneumonia (Non-Covid) infection followed by $(i-p)$ color mapping for class level $L=8$ with activation ξ

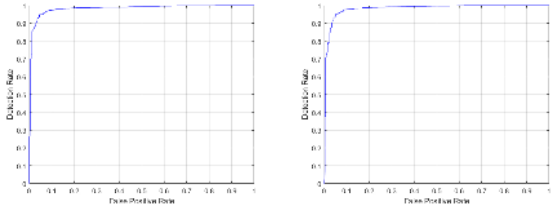

(a) Epochs#5 **(b)** Epochs#10

Figure 9: ROC Curves for the COVID-19 detection rate vs false positive usingthe proposed semi-supervised shallow neural network model

various applications with limited labelled data sets. It remains to investigate the performance of lung CT segmentation using the optimized version of PQIS-Net and the authors are currently engaged in this direction.

References

[1] W. H. O., "Coronavirus disease (COVID-19) pandemic.", https://www.who.int/emergencies/diseases/novel-coronavirus-2019., 2020.

[2] W. H. O., "Coronavirus disease 2019 (COVID-19): Situation report – 123," https://www.who.int/docs/default-source/coronaviruse/situation-reports/20200522-COVID-19-sitrep-123.pdf?sfvrsn=5ad1bc3_4, Accessed May 22, 2020.

[3] L. Fan, D. Li, H. Xue, L. Zhang, Z. Liu, B. Zhang *et al.*, "Progressand prospect on imaging diagnosis of COVID-19", *Chinese Journal of Academic Radiology*, vol. 3, pp. 4—13, 2020, DOI: https://doi.org/10.1007/s42058-020-00031-5.

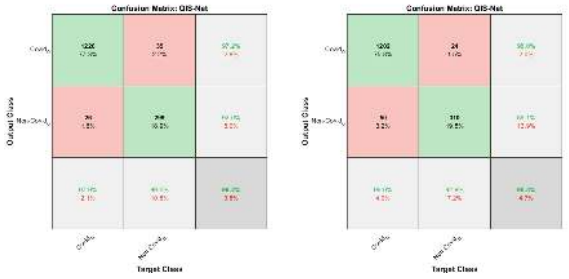

(a) Epochs#5 **(b)** Epochs#10

Figure 10: Confusion matrices for the accuracy of prediction of COVID-19 using proposed semi-supervised shallow neural network model

Table 1: Average Segmentation Accuracy: $ACC = \frac{T_{RP}+T_{RN}}{T_{RP}+F_{LP}+T_{RN}+F_{LN}}$, Dice Similarity: $DS = \frac{2T_{RP}}{2T_{RP}+F_{LP}+F_{LN}}$, $PPV = \frac{T_{RP}}{T_{RP}+F_{LP}}$ and Sensitivity: $SS = \frac{T_{RP}}{T_{RP}+F_{LN}}$ for the data set [30] using PQIS-Net [One sided non-parametric two sample KS test [32] with $\alpha = 0.05$ significance level has been conducted and marked in bold.]

Task	**PQIS-Net**				**3DUNet [10]**				**ResNet50 [9]**			
	ACC	*DS*	*PPV*	*SS*	*ACC*	*DS*	*PPV*	*SS*	*ACC*	*DS*	*PPV*	*SS*
Lung	**0.989**	0.841	**0.793**	**0.972**	**0.990**	**0.871**	**0.799**	0.918	**0.989**	0.853	0.751	0.940
Infection	0.976	0.790	0.741	**0.920**	0.987	0.816	0.734	0.899	**0.989**	**0.833**	**0.774**	0.910
Lung and Infection	**0.988**	0.811	0.773	0.885	**0.990**	**0.852**	0.767	**0.968**	**0.989**	0.819	**0.794**	0.946

Table 2: Performance analyses of the proposed Semi-supervised model, ResNet50 [9], 3D-UNet [10], Kang *et al.* [15] and Wang *et al.* [18] for COVID-19 detection on the Brazilian data set [29] [One sided non-parametric two sample KS test [32] with $\alpha = 0.05$ significance level has been conducted and marked in bold.]

Model	**Accuracy**		**Precision**		**Recall**		**F1-score**		**AUC**	
3D-UNet [10]	0.938	±	**0.893**	±	**0.915**	±	0.817	±	**0.981**	±
	0.081		**0.034**		**0.033**		0.076		0.019	
ResNet50 [9]	**0.949**	±	**0.891**	±	0.894	±	0.815	±	0.978	±
	0.093		**0.180**		0.183		0.039		0.038	
Kang et al. [15]	0.926	±	0.796	±	0.815	±	**0.821**	±	0.938	±
	0.112		0.049		0.057		**0.047**		0.065	
Wang *et al.* [18]	0.939	±	0.810	±	0.897	±	0.818	±	0.940	±
	0.035		0.013		0.097		0.032		0.043	
Proposed Model	0.931	±	**0.890**	±	0.835	±	**0.826**	±	**0.982**	±
	0.139		**0.070**		0.012		**0.021**		**0.027**	

[4] T. Ai, Z. Yang, H. Hou, C. Zhan, C. Chen, W. Lv, Q. Tao, Z. Sun, L. Xia, "Correlation of chest CT and RT-PCR testing in coronavirus disease 2019 (COVID-19) in china: A report of 1014 cases", 2020, https://doi.org/10.1148/radiol.2020200642.

[5] D. Ardila, A. P. Kiraly, S. Bharadwaj, B. Choi, J. J. Reicher, L. Peng, *et al.*, "End-to-end lung cancer screening with three-dimensional deep learning on low-dose chest computed tomography," *Nature Medicine*, vol. 25, pp. 954-–961, 2019, DOI: https://doi.org/10.1038/s41591-019-0447-x.

[6] N. Coudray, P. S. Ocampo, T. Sakellaropoulos, *et al.*, "Classification and mutation prediction from non–small cell lung cancer histopathology images using deep learning," *Nature Medicine*, vol. 24, pp. 1559-–1567, 2018, DOI: https://doi.org/10.1038/s41591-018-0177-5.

[7] F. Liao, M. Liang, Z. Li, X. Hu, and S. Song, "Evaluate the Malignancy of Pulmonary Nodules using the 3-D Deep Leaky Noisy-OR Network," *IEEE Transactions on Neural Networks and Learning Systems*, vol.30, no.11, 2019, DOI: 10.1109/TNNLS.2019.2892409.

[8] H. Zhu, H. Zhao, C. Song, Z. Bian, Y. Bi, T. Liu, X. He, D. Yang, and W. Cai, "MR-Forest: A Deep Decision Framework for False Positive Reduction in Pulmonary Nodule Detection," *IEEE Journal of Biomedical and Health Informatics*, vol. 24, no. 6, 2020, DOI: 10.1109/JBHI.2019.2947506.

[9] B. N. Narayanan, M. S. D. Silva, R. C. Hardie, N. K. Kueterman, R. Ali,"Understanding Deep Neural Network Predictions for Medical Imaging Applications," arXiv:1912.09621, 2019.

[10] J. Ma *et al.*,"Towards Efficient COVID-19 CT Annotation: A Benchmark for Lung and Infection Segmentation,"arXiv:2004.12537, 2020.

[11] L. Li *et al.*, "Artificial Intelligence Distinguishes COVID-19 from Community Acquired Pneumonia on Chest CT,", *Radiology*, 2020, DOI: https://doi.org/10.1148/radiol.2020200905.

[12] D. Singh, V. Kumar, Vaishali, and M. Kaur, "Classification of COVID-19 patients from chest CT images using multi-objective differential evolution–based convolutional neural networks," *European Journal of Clinical Microbiology and Infectious Diseases*, 2020, DOI: https://doi.org/10.1007/s10096-020-03901-z.

[13] S. Roy *et al.*, "Deep learning for classification and localization of COVID-19 markers in point-of-care lung ultrasound," *IEEE Transactions on Medical Imaging*, 2020, DOI: 10.1109/TMI.2020.2994459.

[14] S. Wang *et al.*, "A deep learning algorithm using CT images to screen for coronavirus Disease (COVID-19)," *medRxiv*, 2020, DOI: https://doi.org/10.1101/2020.02.14.20023028.

[15] H. Kangy *et al.*,"Diagnosis of Coronavirus Disease 2019 (COVID-19) with Structured Latent Multi-View Representation Learning," *IEEE Transactions on Medical Imaging*, 2020, DOI:http://dx.doi.org/10.1109/TMI.2020.2992546.

[16] C. Zheng, X. Deng, Q. Fu, and Q. Zhou, "Deep Learning-based Detection for COVID-19 from Chest CT using Weak Label," *MedRxiv*, 2020, DOI: https://doi.org/10.1101/2020.03.12.20027185.

[17] Q. Yan *et al.*, "COVID-19 Chest CT Image Segmentation –A Deep Convolutional Neural Network Solution," https://arxiv.org/abs/2004.10987, 2020.

[18] J. Wang, Y. Bao, Y. Wen, H. Lu, H. Luo, Y. Xiang, X. Li, and C. Liu, "Prior-Attention Residual Learning for More Discriminative COVID-19 Screening in CT Images," *IEEE Transactions on Medical Imaging*, 2020, DOI: 10.1109/TMI.2020.2994908.

[19] D. Konar, S. Bhattacharyya, T. K. Gandhi and B. K. Panigrahi, "A quantum-inspired self-supervised Network model for automatic segmentation of brain MR images," *Applied Soft Computing*, vol. 93, 2020, DOI: https://doi.org/10.1016/j.asoc.2020.106348.

[20] D. Konar, S. Bhattacharyya and B. K. Panigrahi, "QIBDS Net: A Quantum-Inspired Bi-Directional Self-supervised Neural Network Architecture for Automatic Brain MR Image Segmentation," *Proc. 8th International Conference on Pattern Recognition and Machine Intelligence (PReMI 2019)*, vol. 11942, pp. 87–95, 2019, DOI: https://doi.org/10.1007/978-3-030-34872-4_64.

[21] D. Konar, S. Bhattacharyya, S. Dey, and B. K. Panigrahi, "Opti-QIBDS Net: A Quantum-Inspired Optimized Bi-Directional Self-supervised Neural Network Architecture for Automatic Brain MR Image Segmentation," *Proc. 2019 IEEE Region 10 Conference (TENCON)*, pp. 761–766, 2019, DOI: 10.1109/TENCON.2019.8929585.

[22] D. Konar, S. Bhattacharya, U. Chakraborty, T. K.Gandhi, B. K. Panigrahi, "A quantum parallel bi-directional self-organizing neural network (QPBDSONN) architecture for extraction of pure color objects from noisy background", *Proc. IEEE International Conference on Advances in Computing, Communications and Informatics (ICACCI),2016*, pp. 1912–1918, 2016, DOI: 10.1109/ICACCI.2016.7732330.

[23] A. Ghosh, N. R. Pal, and S. K. Pal, "Self organization for object extraction using a multilayer neural network and fuzziness measures," *IEEE Transactions on Fuzzy Systems*, vol. 1, no.1, pp. 54–68, 1993, DOI: 10.1109/TFUZZ.1993.390285.

[24] S. Bhattacharyya, P. Dutta and U. Maulik, "Binary object extraction using bi-directional self-organizing neural network (BDSONN) architecture with fuzzy context sensitive thresholding," *Pattern Anal Applic.*, vol. 10, pp. 345–360, 2007, DOI: https://doi.org/10.1007/s10044-007-0072-z.

[25] S. Bhattacharyya, P. Dutta and U. Maulik, "Multilevel image segmentation with adaptive image context based thresholding", *Applied Soft Computing*, vol. 11, no.1, pp. 946–962, 2011, DOI: https://doi.org/10.1016/j.asoc.2010.01.015.

[26] D. Konar, S. Bhattacharya, B. K. Panigrahi, K. Nakamatsu "A quantum bi-directional self-organizing neural network (QBDSONN) architecture for binary object extraction from a noisy perspective," *Applied Soft Computing*, vol.46, pp. 731–752, 2016, DOI: https://doi.org/10.1016/j.asoc.2015.12.040.

[27] S. Bhattacharyya, P. Pal and S. Bhowmick, "Binary Image Denoising Using a Quantum Multilayer Self Organizing Neural Network," *Applied Soft Computing*, vol.24, pp. 717–729, 2014, https://doi.org/10.1016/j.asoc.2014.08.027.

[28] Y. Oh, S. Park, and J. C. Ye, "Deep Learning COVID-19 Features on CXR using Limited Training Data Sets,", *IEEE Transactions on Medical Imaging*, 2020, DOI: 10.1109/TMI.2020.2993291.

[29] E. Soares, P. Angelov, S. Biaso, M. H. Froes, and D. K. Abe,"SARS-CoV-2 CT-scan dataset: A large dataset of real patients CT scans for SARS-CoV-2 identification," *medRxiv*, 2020, DOI: https://doi.org/10.1101/2020.04.24.20078584.

[30] M. Jun *et al.*, "COVID-19 CT Lung and Infection Segmentation Dataset (Version Verson 1.0) [Data set]," Zenodo.http://doi.org/10.5281/zenodo.3757476, 2020.

[31] T. Fernando, H. Ghaemmaghami, S. Denman, S. Sridharan, N. Hussain, and C. Fookes, "Heart Sound Segmentation Using Bidirectional LSTMs With Attention", *IEEE Journal of Biomedical and Health Informatics*, vol.24, no.6, pp. 1601–1609, 2020, DOI: 10.1109/JBHI.2019.2949516

[32] M. H. Gail and S. B. Green, "Critical values for the one-sided two-sample Kolmogorov–Smirnov statistic," *J. Am. Stat. Assoc.*, vol. 71, pp. 757–760, 1976, DOI: 10.2307/2285616.